Available online at www.sciencedirect.com

ScienceDirect

journal homepage: www.elsevier.com/locate/he

Experimental evaluation and energy analysis of a two-step water splitting thermochemical cycle for solar hydrogen production based on $La_{0.8}Sr_{0.2}CoO_{3-\delta}$ perovskite

M. Orfila [a], M. Linares [a,*], A. Pérez [a], I. Barras-García [b], R. Molina [b], J. Marugán [b], J.A. Botas [a], R. Sanz [b]

[a] Chemical, Energy and Mechanical Technology Department, Rey Juan Carlos University, C/ Tulipán, s/n, 28933, Móstoles, Spain

[b] Chemical and Environmental Technology Department, Rey Juan Carlos University, C/ Tulipán, s/n, 28933, Móstoles, Spain

HIGHLIGHTS

- Commercial perovskite $La_{0.8}Sr_{0.2}CoO_{3-\delta}$ for H_2 production by water splitting.
- Thermal reduction at temperatures >1000 °C led to a loss of cyclability.
- Thermal reduction at 1000 °C preserves the stability of the cobalt oxides.
- High solar to fuel and exergy efficiencies for commercial perovskite $La_{0.8}Sr_{0.2}CoO_{3-\delta}$.

GRAPHICAL ABSTRACT

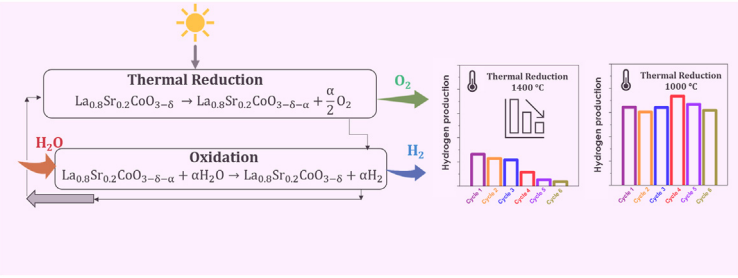

ARTICLE INFO

Article history:
Received 30 July 2021
Received in revised form
2 February 2022
Accepted 9 March 2022
Available online 5 May 2022

Keywords:
Hydrogen production
Thermochemical water splitting
Perovskite

ABSTRACT

A study of the hydrogen production by thermochemical water splitting with a commercial perovskite $La_{0.8}Sr_{0.2}CoO_{3-\delta}$(denoted as LSC) under different temperature conditions is presented. The experiments revealed that high operational temperatures for the thermal reduction step (>1000 °C) implied a decrease in the hydrogen production with each consecutive cycle due to the formation of segregated phases of Co_3O_4. On the other hand, the experiments at lower thermal reduction operational temperatures indicated that the material had a stable behaviour with a hydrogen production of 15.8 cm^3 STP/$g_{material}$·cycle during 20 consecutive cycles at 1000 °C, being negligible at 800 °C. This results comparable or even higher than the maximum values reported in literature for other perovskites (9.80–10.50 STP/$g_{material}$·cycle), but at considerable lower temperatures in the reduction step of the thermochemical cycle for the water splitting (1000 vs 1300–1400 °C). The LSC keeps the

* Corresponding author.
E-mail address: maria.linares@urjc.es (M. Linares).

https://doi.org/10.1016/j.ijhydene.2022.03.077

Exergy analysis
Thermodynamic analysis

perovskite type structure after each thermochemical cycle, ensuring a stable and constant H_2 production. An energy and exergy evaluation of the cycle led to values of solar to fuel efficiency and exergy efficiency of 0.67 and 0.36 (as a percentage of 1), respectively, which are higher than those reported for other metal oxides redox pairs commonly found in the literature, being the reduction temperature remarkably lower. These facts point out to the LSC perovskite as a promising material for full-scale applications of solar hydrogen production with good cyclability and compatible with current concentrating solar power technology.

Symbols and units

Symbol	Meaning	Unit
Δ	Oxygen non-stoichiometry	(–)
A	Extent of reaction	(–)
T_0	Ambient Temperature	(K)
T_{sun}	Effective temperature of the sun	(K)
P_0	Ambient Pressure	(atm)
n_x	Molar Flow of x	(mol/s)
ΔH	Molar Enthalpy variation	(kJ/mol)
ΔS	Molar Entropy variation	(kJ/mol)
λ_{vap}	Latent heat	(kJ/mol)
η_{abs}	Solar absorption efficiency	(–)
$Q_{reactor}$	Required heat in the solar reactor	(kW)
Q_{solar}	Solar heat input	(kW)
$T_{reactor}$	Required T in the solar reactor	(K)
$T_{reduction}$	Required T to perform the reduction reaction	(K)
C	Solar concentration ratio	Suns
I	Direct-normal solar irradiation	(kW/m^2)
Σ	Stefan-Boltzmann constant	(W/m^{2}K^4)
$Q_{reduction}$	Required energy to perform the reduction reaction	(kW)
$Q_{heatingN2}$	Required energy to heat the carrier gas	(kW)
$Q_{steam\ generation}$	Required heat to generate steam	(kW)
$Q_{cooling}$	Released heat in the cooling unit	(kW)
$Q_{condenser}$	Released heat in the condenser unit	(kW)
HHV_{H2}	H_2 higher heating value	(kJ/mol)
Ψ_x	Rate of exergy of x	(kW)
$\Psi_{ch,H2}$	Chemical exergy of H_2	(kJ/mol)
$\eta_{solar\ to\ fuel}$	Solar to fuel efficiency	(–)
ε_{exergy}	Exergy efficiency	(–)

Introduction

Total energy consumption grows every year, and more than 80% of the total energy demand is still covered by fossil fuels such as coal, oil and natural gas. This dependence has important implications: from an economic point of view, the production of fossil fuels is usually located in some regions of the world, which results in volatile and high prices governed by political factors; moreover, the depletion of oil reserves will result in a progressive rise of the prices that will change the overall economic development; from the environmental side, the combustion of the fossil fuels is the leading cause of the greenhouse gases emissions, mainly as CO_2, responsible for the global warming effect to our planet [1,2].

These problems make the situation unsustainable in the medium term, so they have motivated the research of other alternatives as energy sources. Among the different possibilities, hydrogen has been proposed for decades as a very promising energy carrier for a future low carbon energy economy [2,3]. Nowadays, there are many different ways to obtain hydrogen, although most of them do not release the world from fossil fuel dependence [3,4]. Besides, those systems require carbon sequestration to purify the obtained hydrogen, so it is evident that massive use of hydrogen is reasonable only if renewable energy sources are used for its production. However, current renewable energy-based hydrogen production methods are expensive and underdeveloped [5,6].

Thermal splitting of water using concentrated solar energy is the most direct and cleanest method to obtain hydrogen (R1).

$$H_2O \rightarrow H_2 + \frac{1}{2}O_2 \quad \text{(R1)}$$

However, from a practical viewpoint, this reaction is hindered by the high temperature required (>4000 °C) [7], the huge radiation losses which would be proportional to the fourth power of the absolute temperature required and the need to separate the hydrogen and the oxygen to avoid explosive mixtures at lower temperatures [6]. Alternatively, water splitting by solar-driven thermochemical cycles represents a promising technology to deal with these problems.

Thermochemical cycles involve two or more endo- and exothermic reactions, with the net result of the dissociation of water (R1), but with lower temperature requirements than thermal splitting [8]. There are a considerable number of thermochemical cycles reported in the literature [9,10]. Still, those based on two-step redox metal oxides, such as ZnO/Zn, SnO_2/SnO and Fe_3O_4/FeO have been proposed as the most attractive ones for coupling with concentrated solar thermal energy and hydrogen production [8–14]. These

thermochemical cycles involve a first reaction in which the metal oxide is reduced at high temperature releasing oxygen (R2) and a second step in which the reduced metal oxide reacts with water to form H_2 regenerating the initial material (R3) [15,16].

$$MO_{ox} \rightarrow MO_{red} + \frac{1}{2}O_2 \quad \text{(R2)}$$

$$MO_{red} + H_2O \rightarrow MO_{ox} + H_2 \quad \text{(R3)}$$

Despite their simplicity, the temperatures required for the reduction step are still very high (1630–2270 °C), so the researchers have focused their attention on different solutions to decrease this temperature. In this sense, non-stoichiometric oxides have been proposed as potential materials for solar thermal hydrogen production at lower operational temperatures. The advantages of these non-stoichiometric oxides are fast oxidation and reduction kinetics, favourable oxidation thermodynamics, and stability at high temperatures [20–23]. Non-stoichiometric ceria ($CeO_{2-\delta}$) was the first material successfully used in a solar reactor for H_2 production by thermochemical water splitting. However, the degree of non-stoichiometry (δ) that ceria achieves is not large enough to maximize the production of hydrogen [12]. Looking for increasing δ and reducing the reduction temperatures, research efforts have been focused on the study of alternative non-stoichiometric materials for thermochemical cycles. In this context, perovskite oxides have been proposed as potential materials for this purpose for the last ten years [11,17–20].

Perovskites are oxides with ABO_3 or A_2BO_4 type structures (A: large cation, such as La; B: smaller cation, such as Co) that allow the introduction of different metal ions into its structural framework. Moreover, the cation at both A and B sites could be partially substituted by a foreign one (A′ or B′) without destroying the crystalline solid matrix, allowing the creation of oxygen vacancies or the controlled alternation of the oxidation state of cations to keep the electroneutrality [24–26].

The thermochemical water splitting based on perovskites would proceed as follows (R4 and R5) [14]:

$$A_xA'_{1-x}BO_{3-\delta} \rightarrow A_xA'_{1-x}BO_{3-\delta-\alpha} + \frac{\alpha}{2}O_2 \quad \text{(R4)}$$

$$A_xA'_{1-x}BO_{3-\delta-\alpha} + \alpha H_2O \rightarrow A_xA'_{1-x}BO_{3-\delta} + \alpha H_2 \quad \text{(R5)}$$

where δ is the initial defect of oxygen due to the creation of oxygen vacancies and α corresponds to the partial and non-stoichiometric thermal reduction of the perovskite.

A previous work of our research group demonstrated the feasibility of different substituted perovskites for hydrogen production by a two-step thermochemical water splitting cycle performing the reduction step at 1400 °C [28]. The commercial perovskite $La_{0.8}Sr_{0.2}CoO_{3-\delta}$ was revealed as the best material in terms of hydrogen production, but with poor long-term stability. The present work focuses on the evaluation of this material under different operational conditions to ensure its long-term cyclability for stable hydrogen production after subsequent cycles. Additionally, global energy and exergy studies have been carried out to evaluate the performance of the cycle in a model solar thermal facility, confirming this perovskite as an interesting alternative redox material for full-scale applications.

Materials and methods

Materials

Commercial perovskite $La_{0.8}Sr_{0.2}CoO_{3-\delta}$ (LSC) was purchased from Sigma Aldrich. In this material, the large cation (A = La) has been partially substituted by strontium (A' = Sr) so the general structure can be expressed as $A_{1-x}A'_xBO_{3-\delta}$, where δ symbol represents the oxygen vacancies, that is, the non-stoichiometry factor.

Physicochemical characterization

The materials were characterized before and after the thermochemical cycles by different techniques. Crystalline structure was determined by X-Ray diffraction (XRD) using a PW3040/00 X'Pert MPD/MRD (PHILIPS) equipment. Morphology and surface of the materials were observed by Scanning Electron Microscopy (SEM) using a Philips Scanning Electron Microscope XL30 FEG with an accelerating voltage of 5.00 kV and a magnification of 60,000.

Experiments in a high temperature tubular furnace

The thermochemical cycles were carried out on a high temperature tubular furnace coupled to a gas analyser to measure the amount of oxygen and hydrogen released during the reduction and oxidation steps. A Pt/Rh (90/10) crucible was placed inside the furnace as support for 1 g of the perovskite in powder. For the reduction step, temperatures ranging from 1400 to 800 °C were evaluated, maintaining a heating rate of 10 °C/min. A nitrogen flow of 50 NL/h was used as an inert gas carrier to remove the oxygen released from the reaction. For the second step of the cycle, the materials were cooled down to 800 °C, as this temperature is high enough for the oxidation with water (hydrolysis with hydrogen production) according to previous studies [27]. In this step, the nitrogen was saturated in water at 80 °C before feeding the furnace. The N_2 flow is also used as a carrier gas for the hydrogen produced during the oxidation step to a gas analyser model Emerson Xstream. The analyser was previously calibrated using nitrogen as zero gas and 0.5% O_2/N_2 and 0.5% H_2/N_2 as span, respectively. A schematic view of both processes (thermal reduction and oxidation) is shown in the supplementary material (Fig. S1).

Energy and exergy assessment of the process

The comprehensive assessment of the hydrogen production by thermochemical water splitting with LSC requires both energy and exergy analyses. Therefore, a simplified study of the LSC process was simulated for energy and exergy evaluation using the flow diagram depicted in Fig. 1.

The process consists of a solar concentrator, a solar reactor for reduction and oxidation of the perovskite with oxygen and hydrogen production, a cooling unit for the produced oxygen,

and a condensation unit for cooling the hydrogen produced and condensation of the excess of water steam in that stream. The complete cycle was assumed to occur at steady-state and viscous losses, kinetic, and potential energies were neglected. Ideal gases behaviour was assumed. Temperature and pressure of 25 °C and 1 bar were fixed as ambient conditions (T_0 and P_0), respectively and the cycle was calculated for a production of 1 mol/s of H_2.

The thermodynamic properties for H_2, H_2O, O_2, and LSC were extracted from HSC Chemistry 6.0 software from ©Outotec Research Oy. Molar enthalpies and entropies for the reactant and products were determined following standard procedures described elsewhere [27].

The solar reactor was assumed to be a perfectly insulated, blackbody receiver, so the absorption efficiency is given by Eq. (1):

$$\eta_{abs} = \frac{Q_{solar\ reactor}}{Q_{solar}} = 1 - \frac{\sigma \cdot T^4_{solar\ reactor}}{I \cdot C} \quad \text{Eq. (1)}$$

where Q_{solar} is the total solar heat rate input to the cycle (kW), $Q_{solar\ reactor}$ is the total heat needed by the reduction reaction to take place (kW), σ is the Stefan-Boltzmann constant ($5.67 \cdot 10^{-8}$ W/m$^2 \cdot$K^4); $T_{solar\ reactor}$ is the temperature required in the solar reactor, I is the direct-normal solar irradiation taken as 1 kW m^2, and C is the concentration ratio which is defined as the solar radiative flux normalized to 1 kW/m^2 (one *sun* unit).

The initial perovskite material was assumed to be reduced in the solar reactor at a total pressure of 1 atm, up to values of δ and α of 0.03 and 0.22, respectively [27]. The required heat for the reduction is given by Eq. (2) [28]:

$$Q_{reduction} = n_{H_2} \cdot T_{reduction} \cdot \Delta S|_{LSC_{oxidized}@T_0P_0 \rightarrow LSC_{reduced}+\frac{\alpha}{2}O_2@T_{reduction}P_0} \quad \text{Eq. (2)}$$

The released O_2 was continuously removed by the carrier gas. The energy required to heat the carrier gas is described by Eq. (3):

$$Q_{heating N_2} = n_{N_2} \cdot \Delta H|_{N_2@T_0 \rightarrow T_{reduction}} \quad \text{Eq. (3)}$$

Thus, the required heat for the reduction step can be summarised as expressed in Eq. (4):

$$Q_{net\_reduction} = Q_{reduction} + Q_{heating N_2} \quad \text{Eq. (4)}$$

The solar reactor is considered to work adiabatically, so the heat absorbed to carry out the reactions of the first step of the cycle will be leveraged to develop the oxidation with hydrogen generation. Consequently, only thermal reduction will be considered to calculate the total solar heat rate input required in the solar reactor, as it is the limiting step in terms of required temperature and energy. The reduced perovskite leaving the reduction reactor was introduced into the oxidation reactor and mixed with steam. The energy required to generate the steam is also obtained by solar energy, and it is given by Eq. (5):

$$Q_{steam\ gen.} = n_{H_2O} \cdot \left(\Delta H|_{H_2O@T_0 \rightarrow T_{steam\ gen.}} + \lambda_{vap.} + \Delta H|_{H_2O@T_{vap.} \rightarrow T_{oxidizer}} \right) + n_{N_2} \cdot \Delta H|_{N_2@T_0 \rightarrow T_{steam\ gen.}} \quad \text{Eq. (5)}$$

So Q_{solar} is calculated combining Eq. (4) and Eq. (5), from which $Q_{reactor} = Q_{net\_reduction} + Q_{steam\ gen}$, and Eq. (1) as expressed in Eq. (6):

$$Q_{solar} = \frac{Q_{solar\ reactor}}{\eta_{abs}} = \frac{Q_{net\_reduction} + Q_{steam\ gen.}}{\eta_{abs}} = \frac{Q_{reduction} + Q_{heating N_2} + Q_{steam\ gen.}}{\eta_{abs}} \quad \text{Eq. (6)}$$

The solar to fuel efficiency is used as a parameter to compare the potential energy recovery from hydrogen with regards to the solar heat required for its production, and it is calculated according to Eq. (7):

$$\eta_{solar\ to\ fuel} = \frac{n_{H_2} \cdot HHV_{H_2}}{Q_{solar}} \quad \text{Eq. (7)}$$

where HHV_{H2} is the hydrogen higher heating value of 286 kJ/mol [29].

Regarding the exergy, the rate of exergy associated with undiluted thermal radiation from the sun is described by Eq. (8) [30]:

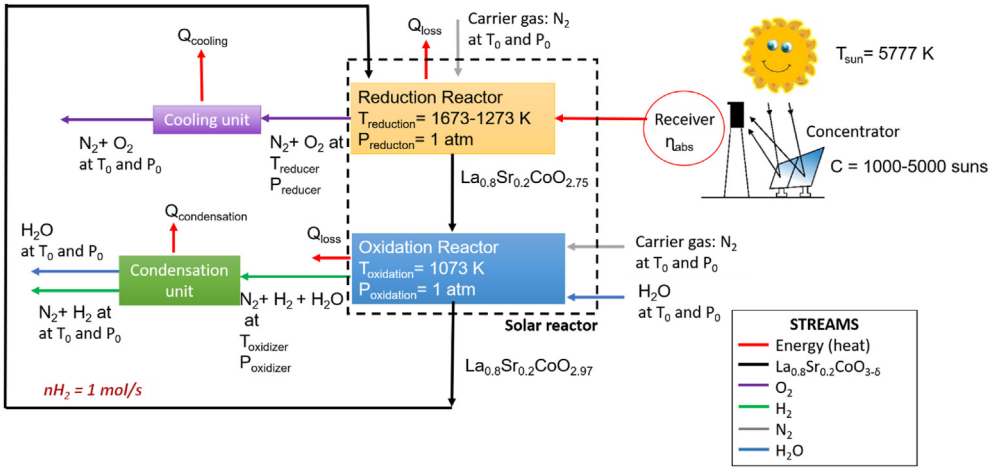

Fig. 1 – Schematic flow diagram of the H_2 production via two-step thermochemical water splitting cycle based on LSC perovskite, including the heat streams of the process.

$$\Psi_{solar} = Q_{solar} \cdot \left(1 - \frac{T_0}{T_{sun}}\right) \quad \text{Eq. (8)}$$

where T_{sun} has a value of 5504 °C, which is considered the effective temperature of the Sun [31].

Finally, exergy efficiency was calculated as a relation between the input energy and the potential electricity generation, assuming that it is produced in a fuel cell fuelling with the hydrogen and with an efficiency of 65% [19,32] (Eq. (9)):

$$\epsilon_{exergy} = \frac{0.65 \cdot n_{H_2} \cdot \Psi_{ch,H_2}}{\Psi_{solar}} \quad \text{Eq. (9)}$$

Variable Ψ_{ch,H_2} in equation Eq. (9) is the chemical exergy of the hydrogen that has an estimated value of 235 kJ/mol [33,34].

According to values of T_0 and T_{sun}, the term in brackets in Eq. (8) achieves a value of 0.94. Thus, Eq. (9) can be simplified to Eq. (10), allowing comparison between the results obtained with the LSC and other energy and exergy analysis reported in the literature for different metallic oxides thermochemical cycles for H_2 production that follows a similar approach [19].

$$\epsilon_{exergy} = \frac{0.65 \cdot n_{H_2} \cdot \Psi_{ch,H_2}}{0.94 \cdot Q_{solar}} = \frac{0.69 \cdot n_{H_2} \cdot \Psi_{ch,H_2}}{Q_{solar}} \quad \text{Eq. (10)}$$

Results and discussion

Study of the reduction temperature

In a previous work, the preliminary evaluation of commercial perovskite $La_{0.8}Sr_{0.2}CoO_{3-\delta}$ (LSC) revealed the LSC perovskite as a promising material for hydrogen production by thermochemical water splitting at temperatures up to 1400 °C for reduction and oxidation steps [27]. However, despite the relevant hydrogen production capacity during the first thermochemical cycle, the material presented a significant decline in subsequent ones. Microscopy analysis showed that the cobalt diffuses to the grain boundaries, creating a very stable segregated phase that is not re-oxidized in the presence of water and reduces the hydrogen production progressively. To improve the thermal stability of the material without decreasing the activity, new cycling experiments were carried outperforming the reduction step at 1400 °C and the oxidation at 800 °C (Fig. 2a–b).

The new oxidation temperature was selected according to the theoretical temperature in which $\Delta G_{oxidation} = 0$ [27]. However, as it can be seen, although the oxidation temperature was significantly lower, the material shows a clear loss of activity along six consecutive cycles. Moreover, the H_2/O_2 molar ratio (varies from 0.4 to 0.1 as the cycles proceed) is far from the theoretical value of 2 expected in a water splitting process, indicating an incomplete reoxidation of the material during reaction with the vapour stream. Consequently, the lack of cyclability and the non-stoichiometrically H_2/O_2 production were critical issues that hindered the suitability of LSC for long-term full-scale applications at those conditions.

The evolution of the crystalline structure of the material along the subsequent cycles was followed by XRD. Results in Fig. 2c show that the main diffraction signals corresponding to the perovskite structure are kept, although they are slightly moved to higher 2θ positions as a result of a distortion of the crystalline network. However, new diffraction signals appear after the first cycle identified as those corresponding to cobalt oxides Co_3O_4 and CoO. Thus, in addition to the distortion of the perovskite structure, new segregated phases appear during the cycles. It should be remarked that oxidation of the Co_3O_4/CoO redox pair is not feasible with water [27,35], so the presence of both species in the LSC after the first cycle would hinder the water splitting process, limiting the hydrogen production of the overall material.

SEM micrographs were taken to assess the evolution of the morphology after each cycle (Fig. 4) and confirm the formation of segregated phases. As it can be seen a significant morphological change is observed after the thermochemical process. The commercial LSC was initially formed by the aggregation of small particles (ca. 100–200 nm), in bigger particles, with sizes around 15–20 μm (Fig. 3a and b). After the consecutive cycles, the small particles and aggregations sinter and agglomerate into bigger macroparticles (Fig. 3c–h), reducing the interface surface and hindering the diffusivity of O_2 and H_2. As the micrographs of the LSC after the cycles were taken by backscattered electrons, they revealed two different phases, especially relevant after the second cycle (Fig. 3d–h). An EDX microanalysis was performed in both phases, confirming different compositions between them. The majority phase corresponds to perovskite, with presence of La, Sr, Co, and O. But the dark spots correspond to a mixture of cobalt oxides clusters, which proportion of ca.72% and 28%, for Co and O, respectively. This fact indicates that, due to the high temperatures suffered by the LSC during the thermochemical cycles, the Co diffuses to the grain boundaries, creating that second phase. The size of the Co oxide clusters seems to be higher with each thermochemical cycle, especially after 5th and 6th ones (Fig. 3g and h).

Diffusion of cations and formation of metallic precipitates have been widely reported in the literature for other perovskite materials exposed to high temperature environments [36,37]. Thus, the material resultant after consecutive thermochemical cycles is different than the initial LSC perovskite. Therefore, additional experimental working at lower temperatures is required to obtain a compromise between activity (H_2 production) and stability under continuous operation in multiple consecutive cycles. A previous thermodynamic study analysing the dependence on temperature of the Gibbs free energy of the thermal reduction of the LSC demonstrated the theoretical temperature necessary for the process was around 1050 °C [27]. In the same study, experimental thermogravimetric measurements revealed that the reduction process efficiently starts at ca. 800–850 °C, if the oxygen is continuously displaced from the LSC.

The influence of reduction temperature in the hydrogen production was then evaluated using lower values in the range from 1200 to 800 °C (Fig. 4). Similarly to 1400 °C, the thermochemical cycles performed at 1200 °C (Fig. 4a) showed a decrease in the oxygen and hydrogen productions in subsequent cycles, even though the final hydrogen production is slightly higher than that obtained at 1400 °C after 6 cycles. This lack of cyclability is also observed when calculating the H_2/O_2 molar ratio obtained in each cycle, as it does not reach values close to 2 (theoretical value for the splitting of the water molecule into oxygen and hydrogen) and change in each cycle

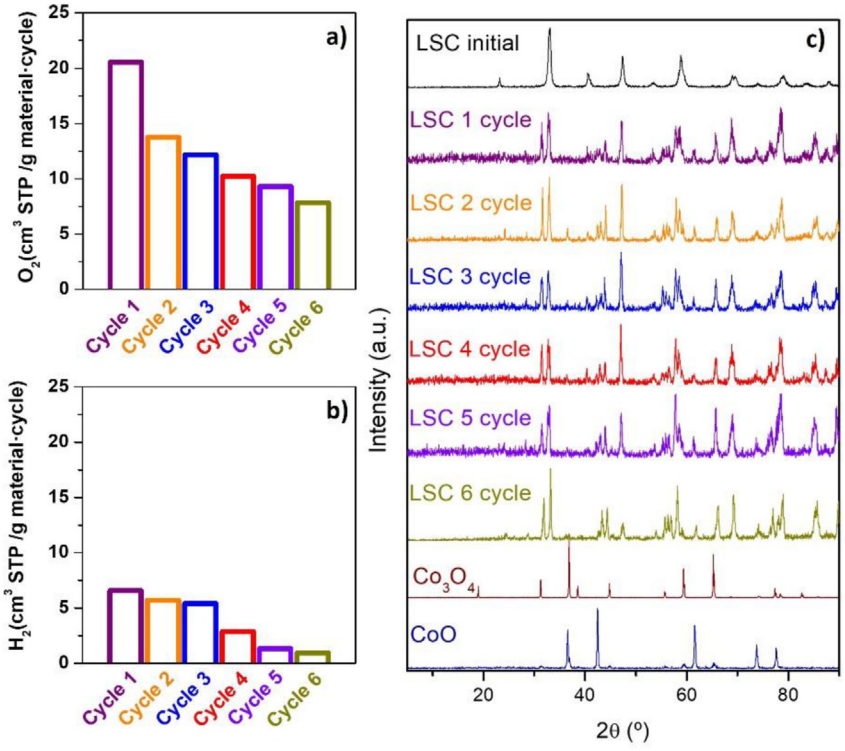

Fig. 2 – a) and b) Oxygen and hydrogen production at thermal reduction at 1400 °C in six consecutive cycles and c) XRD of initial LSC and after each thermochemical cycle.

from 0.45 (1st cycle) to 0.44 (6th cycle). These results demonstrate that the perovskite reduced at 1200 °C, similarly to that reduced at 1400 °C, cannot be totally re-oxidized during the oxidation step, leading to non-stoichiometric productions of hydrogen with respect to the oxygen released during the thermal reduction in each consecutive cycle.

On the contrary, the thermochemical cycle at reduction temperature of 1000 °C (Fig. 4b) allows obtaining a stable release of oxygen and hydrogen production along the six consecutive cycles, with average values in each cycle of 8.64 ± 1.08 cm^3 O_2 STP/$g_{material}$ and 16.31 ± 1.27 cm^3 H_2 STP/$g_{material}$, respectively. However, a further decrease in the thermal reduction to 800 °C (Fig. 4c) produced a negligible hydrogen production, as a consequence of the non-favoured thermal reduction of the LSC materials 800 °C.

These results confirm 1000 °C as optimal temperature for the reduction step, obtaining a hydrogen production between 4 and 9 times higher than the values reported in the literature for other common perovskites like $La_{1-x}Sr_xMnO_{3-\delta}$ (x = 0.5 or 0.35) or $Ba_{1-x}Sr_xCo_{1-y}Fe_yO_{3-\delta}$ (x = 0.25 or 0.5, y = 0.2) [38]. Moreover, the experimental H_2/O_2 molar ratio reached an average value of 1.93 ± 0.31, close to the theoretical value of 2 expected for a water splitting process forming H_2 and O_2. The evolution of the LSC material after each cycle performed at a reduction temperature of 1200 and 1000 °C was evaluated by XRD and SEM techniques. The material after cycles performed isothermally at 800 °C was not characterized, as Fig. 4b demonstrates that the temperature is not enough to promote the thermal reduction of the initial LSC. The XRD patterns corresponding to the commercial perovskite $La_{0.8}Sr_{0.2}CoO_{3-\delta}$ after each cycle at a reduction temperature of 1200 °C show a similar behaviour that the results obtained at 1400 °C (Fig. 2c), showing new diffraction signals after the first cycle corresponding to segregated phases of cobalt oxides Co_3O_4 and CoO. Again, the null capacity of this redox pair to be oxidized with water limits the hydrogen production of the LSC, being this effect more important when the reduction was carried out at a higher temperature.

However, the results at thermal reduction of 1000 °C (Fig. 5b) show that LSC maintains the perovskite structure after each cycle. The diffraction signals are more defined than those obtained with the initial LSC, and new signals diffraction peaks corresponding to cobalt oxides are not detected.

The SEM micrographs obtained after the cycles at 1200 °C (supplementary material, Fig. S2) reveal similar results to those obtained at 1400 °C, being clear the formation of two phases after the 3rd cycle, increasing the contribution of the Co oxide in each cycle. This fact is in accordance with the new signals observed in the XRD patterns. The cobalt oxides phase is very stable and is not re-oxidized in the presence of water [35], explaining the continuous loss of activity of the LSC during the thermochemical cycles at 1400 °C and 1200 °C. In the case of thermochemical cycles performed at a reduction temperature of 1000 °C, the SEM analysis (Fig. 6) reveals a remarkable change in its morphology after the first cycle as compared to the initial LSC (Fig. 3a and b). However, this is a single event effect usually considered as a thermal stabilization of the material during the first high temperature process. This sintering effect is associated with particle densification and coarsening, and the result is an oxide with a characteristic coral-like shape [22]. However, segregated phases are not

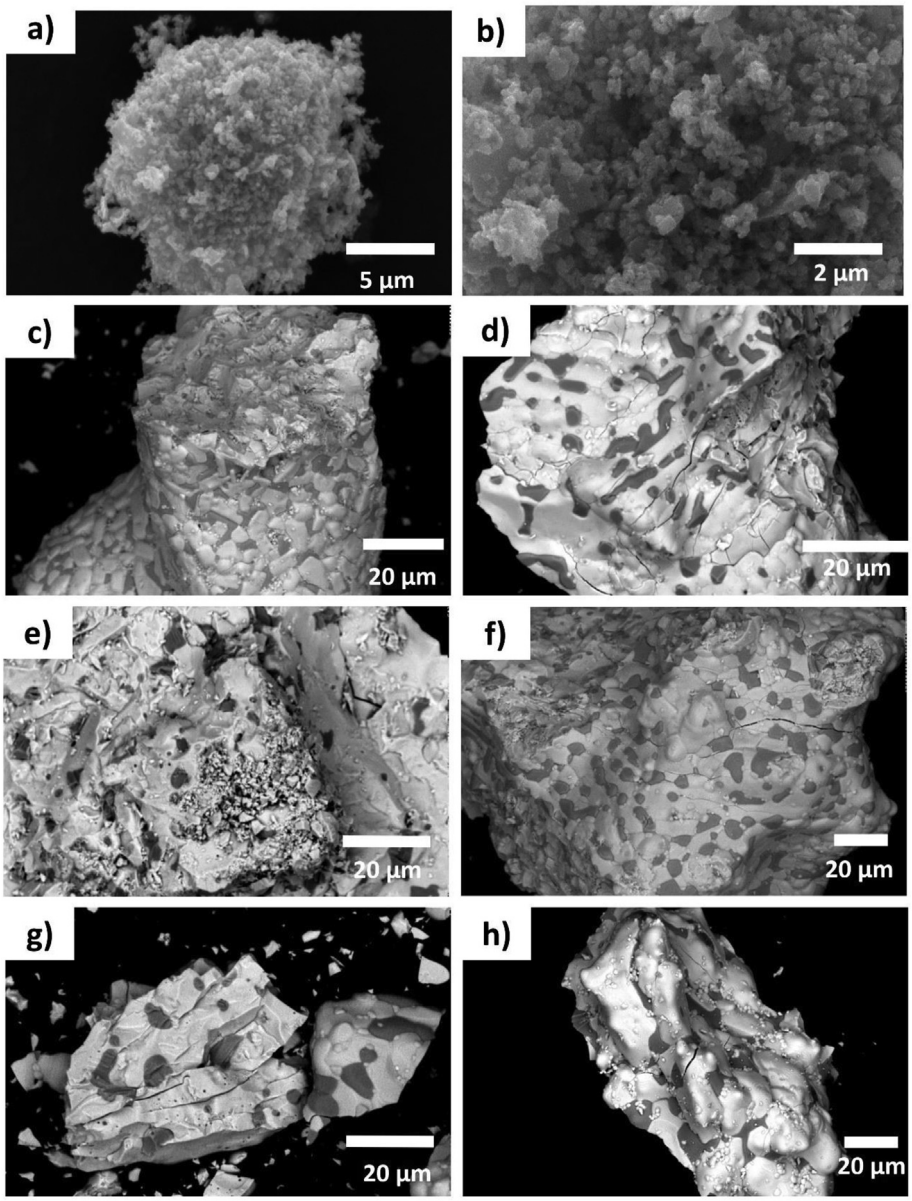

Fig. 3 – SEM micrographs of the commercial LSC: a)-b) micrograph of the initial material, c)-h) micrographs after 1 to 6 consecutive cycles performed at 1400 °C using backscattered electrons.

observed, in contrast with the materials resulting from the thermochemical cycles with reduction steps at 1200–1400 °C (Fig. 3c–h and Fig. S2). Thus, it can be confirmed that performing the reduction step at 1000 °C and the oxidation at 800 °C increases the stability of the material, keeping constant the production of hydrogen along consecutive thermochemical cycles. According to these results, redox properties of the LSC are completely recovered after each cycle, and the segregation and precipitation of cobalt oxides seem to be avoided at this temperature.

Cyclability study of hydrogen production working at 1000 °C for the reduction step

According to the previous section, 1000 °C was selected as an optimal operating temperature for the thermal reduction of the LSC, whereas the rest of variables (nitrogen flow, oxidation temperature, etc.) were maintained. To confirm the good performance data of this material in these conditions, more test cycles were carried out. Fig. 7 shows the H_2 and O_2 productions normalized by mass of LSC obtained in 20 consecutive cycles performed in the high temperature tubular furnace described previously. Additionally, in Fig. 7 are also depicted the average values of the O_2 and H_2 productions as well as the 95% confidence interval. A stable behaviour of the LSC perovskite along the cycles was confirmed. The H_2/O_2 molar ratio remain stable also, around 2, indicating a complete re-oxidation of the material during consecutive cycles. Then regarding the XRD patterns (Fig. S3) obtained after 20 cycles, it can be confirmed the stability of this material.

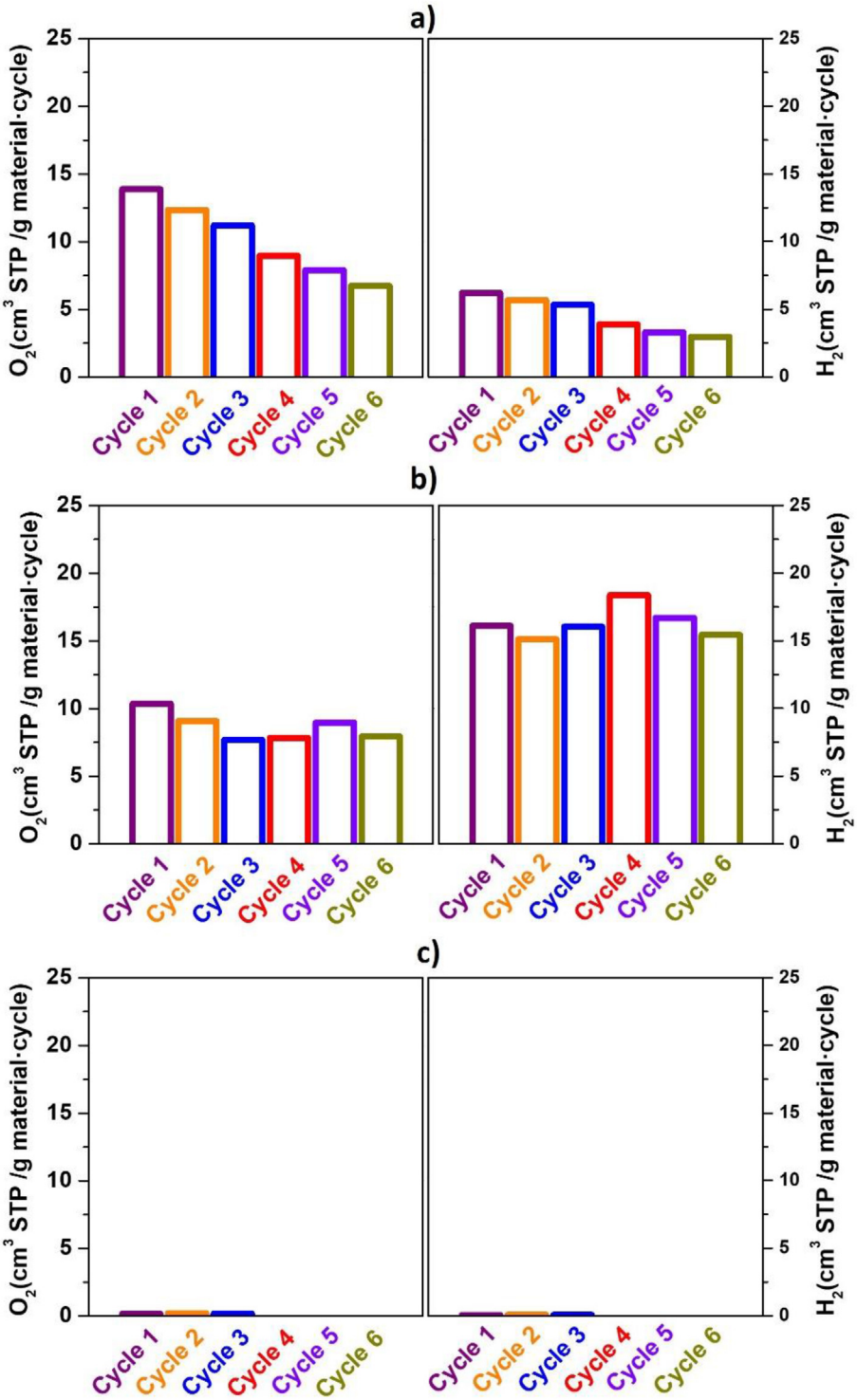

Fig. 4 – O_2 and H_2 production to evaluate the LSC activity in subsequent thermochemical cycles at different reduction temperatures: a) 1200 °C, b) 1000 °C and c) 800 °C. Oxidation at 800 °C (N_2 flow: 50 NL/h, heating rate: 10 °C/min).

Energy and exergy evaluation of the cycle

Once experimentally demonstrated the viability of the commercial perovskite $La_{0.8}Sr_{0.2}CoO_{3-\delta}$ for stable hydrogen production by thermochemical cycles at 1000 °C, the efficiency of the process was evaluated. Solar to fuel efficiency and exergy efficiencies were calculated to evaluate the potential of the cycle for hydrogen production as a way of solar energy storage. The results obtained in the tubular furnace allow the formulation of the following assumptions to perform the calculations of those parameters:

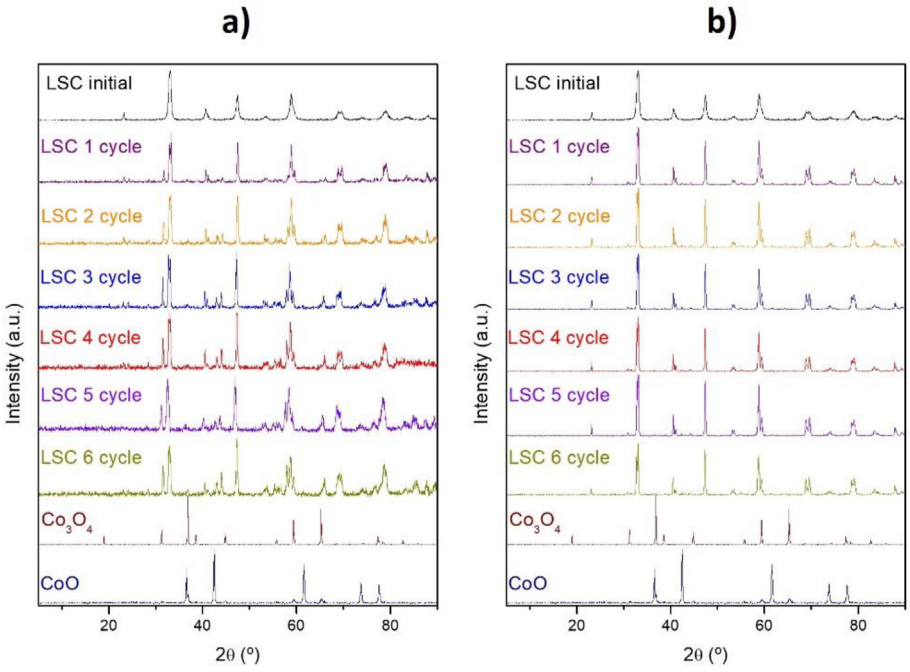

Fig. 5 – XRD of the initial LSC perovskite and after each consecutive cycle at a) 1200 °C, b) 1000 °C.

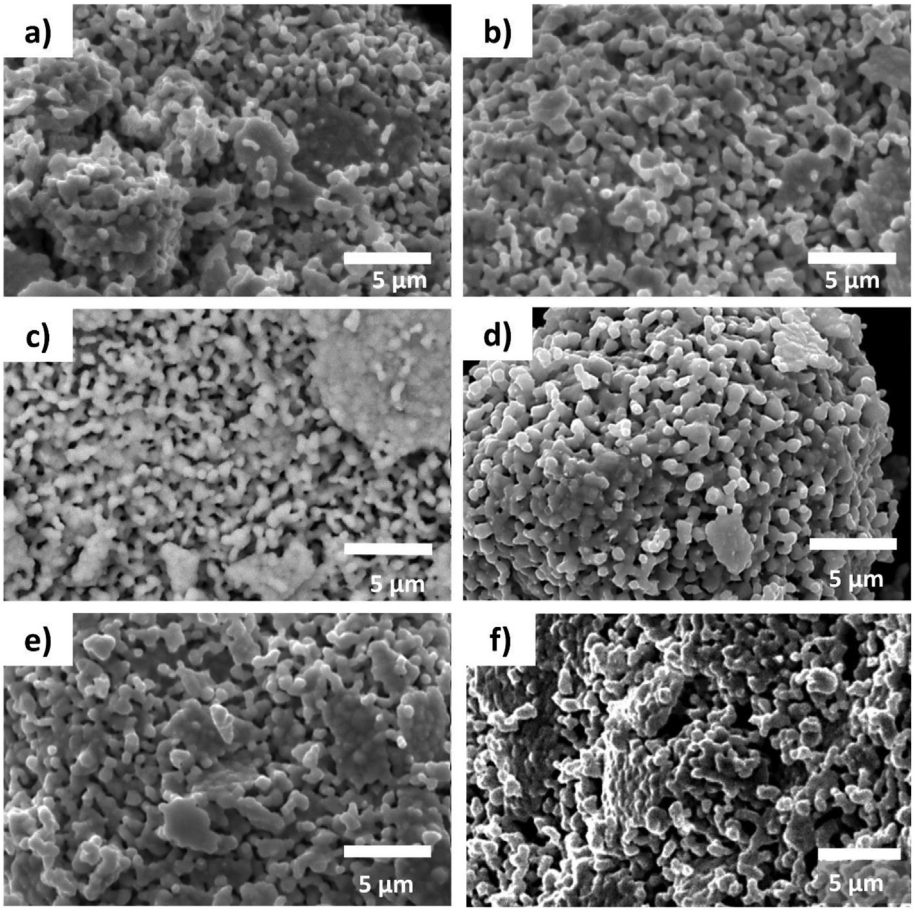

Fig. 6 – SEM micrographs with backscattered electrons of the LSC perovskite after thermochemical cycles performed at 1000 °C: a) 1st cycle, b) 2nd cycle, c) 3rd cycle, d) 4th cycle, e) 5th cycle and f) 6th cycle.

i) The thermal reduction of the LSC is the step with the higher temperature requirements. For that reason, 1000 °C (1273 K), which is the temperature for the thermal reduction that ensures stable operation of the LSC over consecutive cycles, is considered the $T_{reactor}$ for the calculation of absorption efficiency in Eq. (1).

ii) Concentration ratio (C) is critical in this study, as the temperature that can be reached in solar thermal facilities for a constant Q_{solar} is directly related to this parameter. The concentration ratio accounts for optical and geometrical losses in solar concentration systems, and it is often expressed in "suns" units, being the typical values from 1000 to 5000 suns. Although a value of 5000 suns is commonly found in the literature for this kind of energy evaluation [30,31], when C has a higher value means that the concentration capacity is better and higher absorption efficiency is reached in the solar thermal facility (Eq. (1), Fig. S4 in supplementary material). Therefore, the influence of this parameter was evaluated in this study.

iii) According to equation Eq. (6), the heating of the N_2 flow and the generation of water steam for the oxidation of the reduced LSC could require a significant amount of the total heat provided to the reactor. It has been previously established that it is necessary to work experimentally with an excess of inert gas to ensure an inert atmosphere during the reduction step and a good flow of the reaction products [27,40,41]. According to other works, the N_2/H_2 molar ratio has been fixed to a value of 3, being the proportion of carrier gas three times higher than the expected hydrogen production [42]. On the other hand, and due to the stoichiometry of the water splitting reaction, 1 mol/s of water is necessary for a production of 1 mol/s of hydrogen. However, an excess of water could be preferred from an industrial point of view, to ensure complete oxidation of the LSC previously reduced during the previous thermal reduction step. Thus, the influence of the H_2O/H_2 molar ratio from 1 (stoichiometry) to a value of 3 (an excess of 300%) in the solar to fuel and exergy efficiencies was also evaluated.

The results of the efficiency analysis according to these assumptions and the calculations previously described are presented in this section to assess the overall performance of the cycle.

a) Influence of the H_2O/H_2 molar ratio

From the analysis of the results of the energy needed for the process (Table 1), it is evident that heating nitrogen and steam generation requires a considerable amount of the heat flow necessary in the reactor. Depending on the flow ratios, the proportion of energy requested for heating the inert gas and steam generation reach values from 0.37 to 0.51 (as a percentage of 1) of the total heat flow required in the reactor, according to equations Eq. (4) and Eq. (5), at increasing H_2O/H_2 ratio of 1–3, respectively. The heat flow required for steam production is similar to that necessary for heating the N_2 flow in the case of the stoichiometric proportion of water to hydrogen. Still, it raises to 1.8 and 2.6 times higher when increasing the H_2O/H_2 molar ratio to 2 and 3, respectively. Consequently, this molar ratio has a critical influence on the heat flow that the solar thermal facility should concentrate to promote the thermochemical water splitting with the LSC perovskite or Q_{solar} (supplementary material, Fig. S5). Therefore, this molar ratio impacts the *solar to fuel* and *exergy efficiencies* achieved values (Fig. 8).

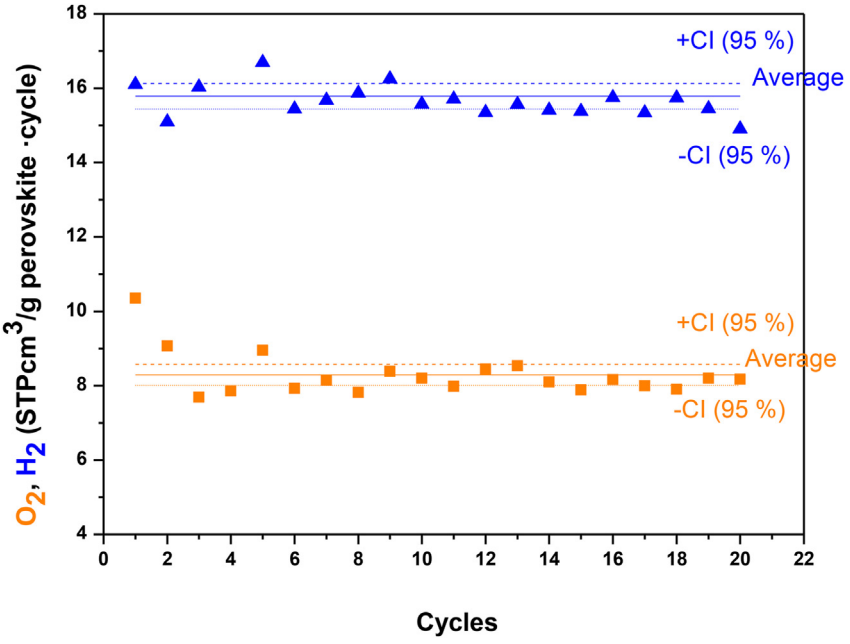

Fig. 7 – Performance of the LSC material in 20 consecutive thermochemical cycles: amount of released oxygen at 1000 °C and total amount of released hydrogen at 800 °C (N_2 flow: 50 NL/h, heating rate: 10 °C/min).

Table 1 – Heat flows necessary for reduction, heating N_2 flow, and steam generation as a function of the H_2O/H_2 molar ratio at a constant N_2/H_2 ratio of 3.

H_2O/H_2 molar ratio	$Q_{reduction}$ (kW)	$Q_{heating\ N2}$ (kW)	$Q_{steam\ generation}$ (kW)
1	312.04	92.39	96.5
2			169.6
3			242.6

The heat flow required for steam production increases remarkably with the H_2O/H_2 molar ratio. This parameter has more influence in Q_{solar} than the solar concentration ratio because in this case, the absorption efficiencies are very high (Fig. S4), so the differences between C = 3000 suns or C = 5000 suns are not significant (Fig. S5). These results indicate that thermochemical hydrogen production is feasible with current solar concentration facilities like central tower plants or parabolic dishes, in which current values for C up to 3000 are possible [15].

On the other hand, it is evident that the higher the amount of water, the lower both solar to fuel and exergy efficiencies, due to the increase in the energy requirements. The solar to fuel efficiency decreases between 0.08 and 0.16 when H_2O/H_2 molar ratio goes from 1 to 3, while the exergy efficiency decreases between 0.04 and 0.08. For each H_2O/H_2 ratio, the effect of C is negligible between 2000 and 5000 suns, although both parameters increase around 0.03–0.05 when C increases from 1000 to 2000 suns.

b) Effect of partial heat recovery from the products streams

The results of exergy and solar to fuel efficiencies showed previously were calculated based on the energy requirements for the thermochemical process, heating the carrier gas, and generation of steam. However, exergy associated with the oxygen and hydrogen flows coming from the solar reactor in each step were not considered. The energy associated with both flows could be partially recovered to contribute to the energy requirements of the overall system. For example, it can be used for pre-heating the N_2 stream before entering the reactor or pre-heating the H_2O flow before the oxidation reactor.

The oxygen released during the thermal reduction of the LSC is continuously removed from the reduction reaction beside the carrier gas and cooled down to ambient temperature. Thus, the heat rejected in the cooling unit can be calculated as shown in Eq. (11):

$$Q_{cooling} = n_{O_2\_released} \cdot \Delta H|_{O_2@T_{reduction} \rightarrow T_0} + n_{N_2} \cdot \Delta H|_{N_2@T_{reduction} \rightarrow T_0} \quad \text{Eq. (11)}$$

On the other hand, the mixture of hydrogen, unreacted vapour, and nitrogen from the oxidation reactor goes through a condenser to separate the water from the hydrogen, reaching at the end of the process ambient temperature. The theoretical heat released in this unit could be obtained by Eq. (12):

$$Q_{condenser} = n_{H_2} \cdot \Delta H|_{H_2@T_{oxidation} \rightarrow T_0} + n_{H_2O\_excess} \cdot \left(\Delta H|_{H_2O@T_{oxidation} \rightarrow T_{cond.}} + \lambda_{cond.} + \Delta H|_{H_2O@T_{cond.} \rightarrow T_0}\right) + n_{N_2} \cdot \Delta H|_{N_2,@T_{oxidation} \rightarrow T_0} \quad \text{Eq. (12)}$$

Assuming an efficiency of 70% in the heat recovery systems [19], the energy recovered from the cooling unit and the condenser after the reduction and oxidation reactors at different water to hydrogen molar ratios are shown in Table 2. Comparing these results with those shown in Table 1, the heat recovery accounts for 0.28 to 0.38 (as a percentage of 1) of the total heat required in the process, which a considerable energy saving in the system. A scenario in which up to 70% of the

Table 2 – Recovered heat assuming 70% of efficiency in the heat recovery systems.

H_2O/H_2 molar ratio	$Q_{cooling\ unit}$ (kW)	$Q_{condenser}$ (kW)	$\sum Q_{recovered}$ (kW)
1	−74.70	−64.92	−139.61
2		−116.03	−190.73
3		−167.15	−241.85

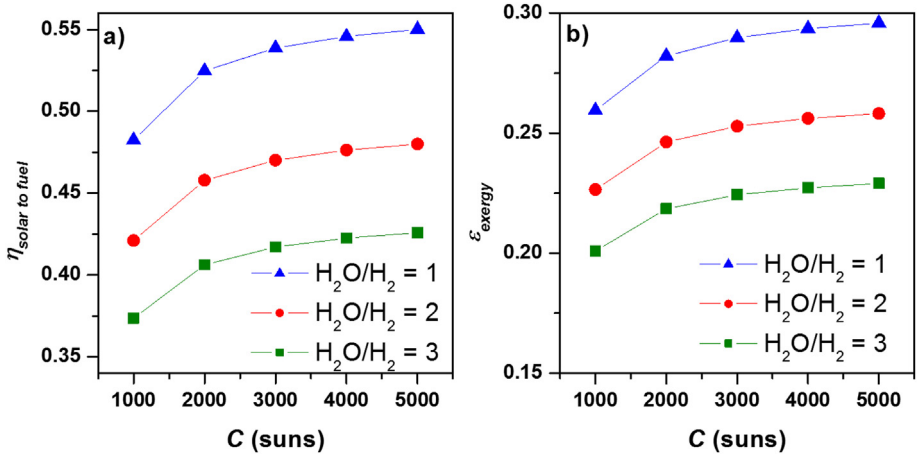

Fig. 8 – a) Solar to fuel efficiency and b) exergy efficiency as a function of the solar concentration ratio for different H_2O/H_2 molar ratios (N_2/H_2 = 3).

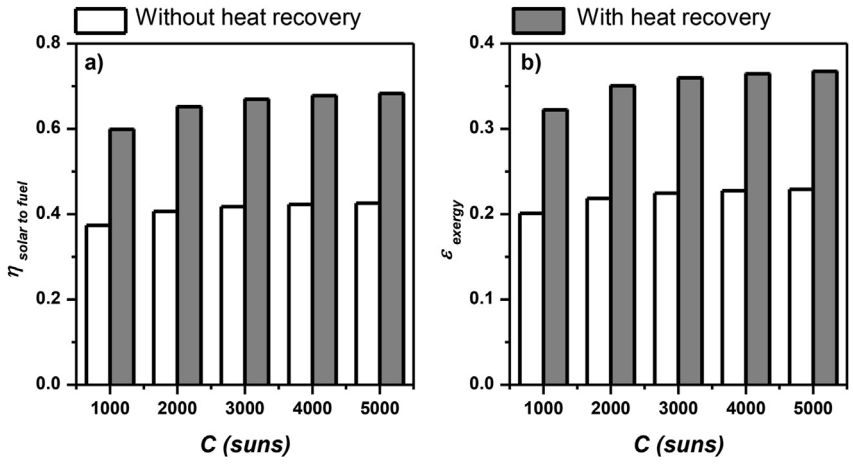

Fig. 9 – Comparison of a) Solar to fuel efficiency and b) exergy efficiency in presence and absence of heat recovery systems, and as a function of the solar concentration ratio for $H_2O/H_2 = 3$.

energy associated with the heat of the gas products from the oxidation and the reduction can be used for pre-heating the reactants produces a dramatic increase in the solar to fuel and exergy efficiencies of the system. Values for both parameters for different concentration factors and H_2O/H_2 molar ratios are shown in supplementary material (Fig. S6), being the comparison between scenarios in absence and presence of heat exchanger systems for a H_2O/H_2 molar ratio of 3 represented in Fig. 9. This molar ratio has been chosen as the worst-case scenario in terms of energy demanded for the thermochemical cycle for water splitting. But, even in this case, the results revealed an increase in the solar to fuel and exergy efficiencies of 0.58 in case of heat recovery, as compared to the results obtained in absence of heat exchangers.

Taking these results into account, it is evident that it is necessary to take advantage of the released heat flows in the cooling units to heat the carrier gas and generate the steam to improve both solar to fuel and exergy efficiencies of the cycle.

c) Comparison with other two steps metal oxide thermochemical cycles

A few years ago, Yadav and Banerjee published a review summarizing the results obtained in the thermodynamic comparison of different metal oxide redox pair based thermochemical cycles for hydrogen production [19]. Solar to fuel and exergy efficiencies were calculated assuming a value of $C = 5000$ suns, and following a procedure close to that used in this work, assuming an energy recovery of 70% from the products streams. The only difference was that the exergy for hydrogen in equation Eq. (10) (ψ_{ch,H_2}) is substituted by the Gibbs free energy for $\Delta G_{H_2+1/2O_2\rightarrow H_2O}$, with a value of 237.2 kJ/mol instead of 235 kJ/mol. More recently, the authors expanded that study, including other materials based on mixed metal oxides for thermochemical water splitting, such as Mn_2O_3/MnO or $Mn_xCo_yO_4$ spinels [32,42]. The comparison of the results obtained in those studies with the current calculations obtained with the commercial LSC material is shown in Fig. 10. Both the solar to fuel efficiency and the exergy efficiency of the thermochemical cycle based on the LSC material are higher than others reported in the literature. Results are comparable to those obtained for the ZnO/Zn thermochemical cycle but at a significantly lower reduction

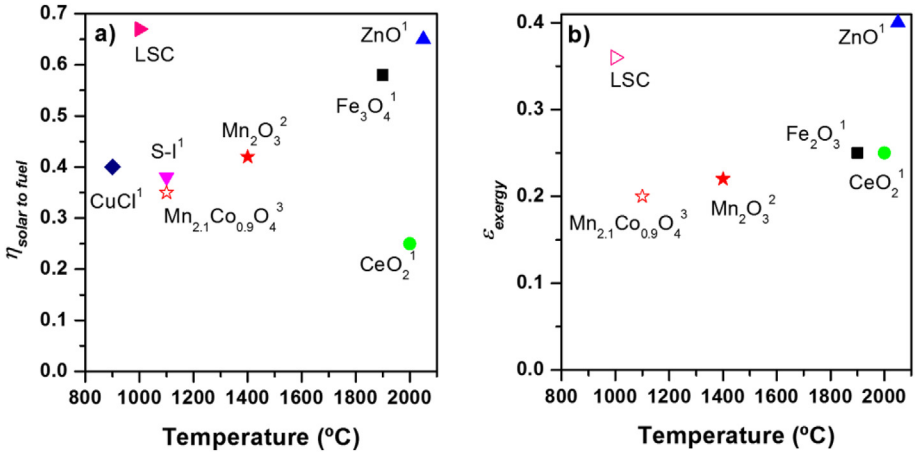

Fig. 10 – Comparison of a) Solar to fuel efficiency and b) exergy efficiency for LSC and other thermochemical cycles ([1]values taken from Ref. [19], [2]value taken from Ref. [42] and [3]value taken from Ref. [32]).

temperature. Additionally, both efficiencies were higher than the obtained with the CeO_2, reference material for this kind of process. It is especially remarkable the solar to fuel efficiency obtained with the LSC, more than two times higher than that of the ceria redox cycle. These results confirm the LSC perovskite as a very promising material for a full-scale H_2 production by solar driven thermochemical cycle.

Conclusions

The strong dependence of the cyclability of the commercial perovskite $La_{0.8}Sr_{0.2}CoO_{3-\delta}$ under different operational conditions has been assessed. The experimental results for hydrogen production on a high temperature tubular furnace showed that thermal reduction at 1200 °C or 1400 °C led to a loss of cyclability with a significant decrease in the hydrogen production from 6.25 cm^3 STP $H_2/g_{material}$ to 1 cm^3 STP $H_2/g_{material}$ after six cycles for the higher temperature. The characterization of the LSC after the process showed the segregation of Co and the formation of cobalt oxides precipitates. The stability of the cobalt oxides towards the thermal reduction and oxidation with water seems to be the main responsible for the loss of activity of the LSC at 1200 °C and 1400 °C.

In contrast, when the thermal reduction step is conducted at 1000 °C, a stable hydrogen production of 15.8 cm^3 STP/$g_{material}$·cycle was obtained during 20 consecutive cycles. This value is higher than those found in the literature for other perovskites (usually 10 cm^3 STP performing the reduction at 1300–1400 °C and the oxidation at 1000 °C). This lower temperature avoids the segregation of the metallic cation to the boundary grain and the formation of stable cobalt oxides. Thus, LSC material is completely recovered after each thermochemical cycle, maintaining the hydrogen production along with the cycles.

The thermodynamic evaluation of the process revealed higher solar to fuel and exergy efficiencies than those obtained for other materials reported in the literature, and the operation temperature is remarkably lower. Consequently, the LSC is a promising redox material for full-scale hydrogen thermochemical water splitting applications using solar concentration facilities.

Declaration of competing interest

The authors declare that they have no known competing financial interests or personal relationships that could have appeared to influence the work reported in this paper.

Acknowledgements

The authors thank "Universidad Rey Juan Carlos", "Comunidad de Madrid" and European Structural Funds for their financial support to SOLTOCOMB Young Researchers R&D Project (Ref. M – 2174) and ACES2030-CM Project (S2018/EMT-4319).

Appendix A. Supplementary data

Supplementary data to this article can be found online at https://doi.org/10.1016/j.ijhydene.2022.03.077.

REFERENCES

[1] BP. BP statistical review of world energy. 2021.
[2] International Energy Agency. Global energy review 2021. Glob Energy Rev 2021;2020:1–36. Available, https://iea.blob.core.windows.net/assets/d0031107-401d-4a2f-a48b9eed19457335/GlobalEnergyReview2021.pdf.
[3] Roeb M, Monnerie N, Houaijia A, Thomey D, Sattler C. Chapter 4 - solar thermal water splitting. Elsevier; 2013.
[4] Ishaq H, Dincer I, Crawford C. A review on hydrogen production and utilization: challenges and opportunities. Int J Hydrogen Energy 2022;47(62):26238–64. https://doi.org/10.1016/j.ijhydene.2021.11.149.
[5] Nikolaidis P, Poullikkas A. A comparative overview of hydrogen production processes. Renew Sustain Energy Rev 2017;67:597–611. https://doi.org/10.1016/j.rser.2016.09.044.
[6] Yilmaz F, Balta MT, Selbaş R. A review of solar based hydrogen production methods. Renew Sustain Energy Rev 2016;56:171–8. https://doi.org/10.1016/j.rser.2015.11.060.
[7] W. J. Martinez-Burgos E. de Souza Candeo, A. B. Pedroni Medeiros, J. C. de Carvanho, V. Oliveira de Andrade Tanobe, C. R. Soccol, and E. B. Sydney, "Hydrogen: current advances and patented technologies of its renewable production," J Clean Prod, vol. 286, 2021, doi: 10.1016/j.jclepro.2020.124970.
[8] Agrafiotis C, Roeb M, Sattler C. A review on solar thermal syngas production via redox pair-based water/carbon dioxide splitting thermochemical cycles. Renew Sustain Energy Rev 2015;42:254–85. https://doi.org/10.1016/j.rser.2014.09.039.
[9] Muhich CL, Blaser S, Hoes MC, Steinfeld A. Comparing the solar-to-fuel energy conversion efficiency of ceria and perovskite based thermochemical redox cycles for splitting H_2O and CO_2. Int J Hydrogen Energy 2018;43(41):18814–31. https://doi.org/10.1016/j.ijhydene.2018.08.137.
[10] Mao Y, Gao Y, Dong W, Wu H, Song Z, Zhao X, Sun J, Wang W. Hydrogen production via a two-step water splitting thermochemical cycle based on metal oxide – a review. Appl Energy 2020;267:114860. https://doi.org/10.1016/j.apenergy.2020.114860.
[11] Roeb M, Neises M, Monnerie N, Call F, Simon H, Sattler C, Schmücker M, Pitz-Paal R. Materials-related aspects of thermochemical water and carbon dioxide splitting: a review. Materials 2012;5(11):2015–54. https://doi.org/10.3390/ma5112015.
[12] Bayon A, de la Calle A, Ghose KK, Page A, McNaughton R. Experimental, computational and thermodynamic studies in perovskites metal oxides for thermochemical fuel production: a review. Int J Hydrogen Energy 2020;45(23):12653–79. https://doi.org/10.1016/j.ijhydene.2020.02.126.
[13] Furler P, Scheffe JR, Gorbar M, Moes L, Vogt U, Steinfeld A. Solar thermochemical CO_2 splitting using a reticulated porous ceria redox system. Energy Fuels 2012;26:7051–9. https://doi.org/10.1021/ef3013757.
[14] Scheffe JR, Weibel D, Steinfeld A. Lanthanum–strontium–Manganese perovskites as redox materials for solar thermochemical splitting of H_2O and CO_2. Energy Fuels 2013;27(8):4250–7. https://doi.org/10.1021/ef301923h.

[15] Jin J, Fu M, Wang L, Ma T, Li X, Ji F, Lu Y. Water-splitting mechanism analysis of Sr/Ca doped $LaFeO_3$ towards commercial efficiency of solar thermochemical H_2 production. Int J Hydrogen Energy 2021;46(2):1634–41. https://doi.org/10.1016/j.ijhydene.2020.10.033.
[16] Barcellos RD, Sanders MD, Tong J, McDaniel AH, O'Hayre RP. BaCe0.25Mn0.75O3-: δ - promising perovskite-type oxide for solar thermochemical hydrogen production. Energy Environ Sci 2018;11(11):3256–65. https://doi.org/10.1039/c8ee01989d.
[17] Oruc O, Dincer I. Assessing the potential of thermochemical water splitting cycles: a bridge towards for clean and sustainable hydrogen generation. Fuel 2021;286(P2):119325. https://doi.org/10.1016/j.fuel.2020.119325.
[18] Steinfeld A. Solar thermochemical production of hydrogen - a review. Sol Energy 2005;78(5):603–15. https://doi.org/10.1016/j.solener.2003.12.012.
[19] Yadav D, Banerjee R. A review of solar thermochemical processes. Renew Sustain Energy Rev 2016;54:497–532. https://doi.org/10.1016/j.rser.2015.10.026.
[20] Haeussler A, Abanades S, Julbe A, Jouannaux J, Cartoixa B. Two-step CO_2 and H_2O splitting using perovskite-coated ceria foam for enhanced green fuel production in a porous volumetric solar reactor. *J CO_2 Util* 2020;41(July):101257. https://doi.org/10.1016/j.jcou.2020.101257.
[21] Şanlı SB, Pişkin B. Effect of B-site Al substitution on hydrogen production of $La_{0.4}Sr_{0.6}Mn_{1-x}Al_x$ (x=0.4, 0.5 and 0.6) perovskite oxides. Int J Hydrogen Energy 2022;47(45):19411–21. https://doi.org/10.1016/j.ijhydene.2021.12.047.
[22] Pein M, Agrafiotis C, Vieten J, Brendelberger S, Roeb M, Sattler C. Redox thermochemistry of Ca-Mn-based perovskites for oxygen atmosphere control in solar-thermochemical processes. Sol Energy 2020;198:612–22. https://doi.org/10.1016/j.solener.2020.01.088.
[23] Gokon N, Hara K, Sugiyama Y, Bellan S, Kodama T, Hyun-seok C. Thermochemical two-step water splitting cycle using perovskite oxides based on $LaSrMnO_3$ redox system for solar H_2 production. Thermochim Acta 2019;680:178374. https://doi.org/10.1016/j.tca.2019.178374.
[24] Ngoensawat A, Tongnan V, Laosiripojana N, Kim-Lohsoontorn P, Hartley UW. Effect of La and Gd substitution in $BaFeO_{3-\delta}$ perovskite structure on its catalytic performance for thermochemical water splitting. Catal Commun 2020;135:105901. https://doi.org/10.1016/j.catcom.2019.105901.
[25] Zhu J, Thomas A. Perovskite-type mixed oxides as catalytic material for NO removal. Appl Catal B Environ 2009;92(3–4):225–33. https://doi.org/10.1016/j.apcatb.2009.08.008.
[26] Pérez A, Orfila M, Linares M, Sanz R, Marugán J, Molina R, et al. Hydrogen production by thermochemical water splitting with $La_{0.8}Al_{0.2}MeO_{3-\delta}$ (Me= Fe, Co, Ni and Cu) Perovskites prepared under controlled pH. Catal Today 2022;390-391:22–33. https://doi.org/10.1016/j.cattod.2021.12.014.
[27] Orfila M, Linares M, Molina R, Botas JÁ, Sanz R, Marugán J. Perovskite materials for hydrogen production by thermochemical water splitting. Int J Hydrogen Energy Nov. 2016;41(42):19329–38. https://doi.org/10.1016/J.IJHYDENE.2016.07.041.
[28] Fletcher EA, Noring JE. High temperature solar electrothermal processing-Zinc from zinc oxide. Energy 1983;8(4):247–54. https://doi.org/10.1016/0360-5442(83)90100-7.
[29] Nixon A, Ferrandon M, Kaye MH, Trevani L. Thermochemical production of hydrogen. Woodhead Publishing Limited; 2011.
[30] Petela R. Exergy of undiluted thermal radiation. Sol Energy 2003;74(6):469–88. https://doi.org/10.1016/S0038-092X(03)00226-3.
[31] Parrott JE. Choice of an equivalent black body solar temperature. Sol Energy 1993;51(3):195.
[32] Orfila M, Linares M, Molina R, Marugán J, Botas JA, Sanz R. Hydrogen production by water splitting with $Mn_{3-x}Co_xO_4$ mixed oxides thermochemical cycles: a thermodynamic analysis. Energy Convers Manag 2020;216:112945. https://doi.org/10.1016/j.enconman.2020.112945.
[33] Schieber GL, Stechel EB, Ambrosini A, Miller JE, Peter G. H_2O splitting via a two-step solar thermoelectrolytic cycle based on non-stoichiometric ceria redox reactions : thermodynamic analysis George W . Woodruff School of Mechanical Engineering , Georgia Institute of Technology , Atlanta , Corresponding Autho. Int J Hydrogen Energy 2017;42(30):18785–93.
[34] Weinstein LA, Loomis J, Bhatia B, Bierman DM, Wang EN, Chen G. Concentrating solar power. Chem Rev 2015;115(23):12797–838. https://doi.org/10.1021/acs.chemrev.5b00397.
[35] Orfila M, Linares M, Molina R, Botas JA, Marugán J, Sanz R. Thermochemical hydrogen production using manganese cobalt spinels as redox materials. Int J Hydrogen Energy 2017;42(19). https://doi.org/10.1016/j.ijhydene.2017.02.027.
[36] Wei B, Schroeder M, Martin M. Surface cation segregation and chromium deposition on the double-perovskite oxide $PrBaCo_2O_{5+\delta}$. Feb. 2018. https://doi.org/10.1021/acsami.7b17881.s001.
[37] Li Y, Zhang W, Zheng Y, Chen J, Yu B, Chen Y, Liu M. Controlling cation segregation in perovskite-based electrodes for high electro-catalytic activity and durability. Chem Soc Rev 2017;46(20):6345–78. https://doi.org/10.1039/C7CS00120G.
[38] Abanades S. Metal oxides applied to thermochemical water-splitting for hydrogen production using concentrated solar energy. ChemEng 2019;3(3):63. https://doi.org/10.3390/chemengineering3030063.
[40] Weinstein LA, Loomis J, Bhatia B, Bierman DM, Wang EN, Chen G. Concentrating solar power. Chem Rev 2015;115(23):12797–838. https://doi.org/10.1021/acs.chemrev.5b00397.
[41] Marugán J, Botas JA, Martín M, Molina R, Herradón C. Study of the first step of the Mn_2O_3/MnO thermochemical cycle for solar hydrogen production. Int J Hydrogen Energy 2012;37(8). https://doi.org/10.1016/j.ijhydene.2011.10.124.
[42] Herradón C, Molina R, Marugán J, Botas JÁ. Experimental assessment of the cyclability of the Mn_2O_3/MnO thermochemical cycle for solar hydrogen production. Int J Hydrogen Energy Jan. 2019;44(1):91–100. https://doi.org/10.1016/J.IJHYDENE.2018.06.158.